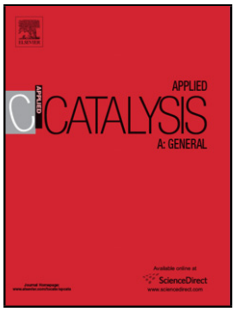

Title: Synthesis of ethyl lactate from triose sugars on Sn/Al_2O_3 catalysts

Author: E. Pighin V.K. Díez J.I.Di Cosimo

PII: S0926-860X(16)30117-X
DOI: http://dx.doi.org/doi:10.1016/j.apcata.2016.03.007
Reference: APCATA 15799

To appear in: *Applied Catalysis A: General*

Received date: 5-1-2016
Revised date: 26-2-2016
Accepted date: 8-3-2016

Please cite this article as: E.Pighin, V.K.Díez, J.I.Di Cosimo, Synthesis of ethyl lactate from triose sugars on Sn/Al2O3 catalysts, Applied Catalysis A, General http://dx.doi.org/10.1016/j.apcata.2016.03.007

Submitted to Appl. Catal. A General, January 2016. Revised version, February, 2016.

Synthesis of ethyl lactate from triose sugars on Sn/Al_2O_3 catalysts

E. Pighin, V.K. Díez and J.I. Di Cosimo*

Catalysis Science and Engineering Research Group (GICIC), INCAPE, UNL-CONICET, CCT CONICET Santa Fe, Colectora Ruta Nac. 168, km 0, Paraje "El Pozo", (3000) Santa Fe, Argentina

*Corresponding author. Tel.: +54 342 4511546 , Ex 6118; Fax: +54 342 4511170.
E-mail address: dicosimo@fiq.unl.edu.ar (J.I. Di Cosimo).

Graphical abstract

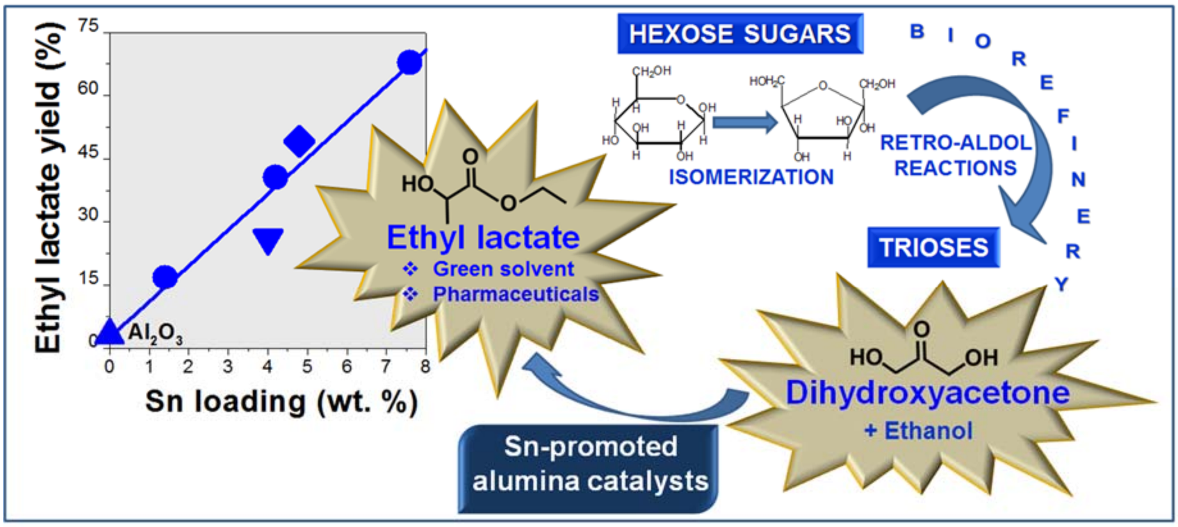

Highlights:

- Inexpensive and easily scalable alumina-supported Sn catalysts with different Sn loadings promote ethyl lactate formation from triose sugars and ethanol.
- Ethyl lactate yields of ≈70% are obtained on a 7.6 wt.% Sn/Al$_2$O$_3$ catalyst at 353K.
- Catalyst preparation conditions, Sn content and reaction conditions affect the final ethyl lactate yield.
- Surface Lewis acid sites that increase with Sn loading participate in the kinetically relevant reaction steps.

Abstract

Sn-promoted alumina catalysts with different Sn loadings (1-8 wt.%) were prepared by impregnation and characterized by N$_2$ physisorption, X-ray diffraction, UV-vis-DRS, FTIR of pyridine and TPD of NH$_3$. Surface Sn species present Lewis acid properties different from those of the alumina support; the number and strength of the surface

Lewis centers increase with the Sn loading. These materials exhibit good catalytic performance for conversion of triose sugars, such as dihydroxyacetone, toward ethyl lactates at mild conditions. The catalyst preparation conditions, Sn content and reaction conditions affect the final ethyl lactate yield. Yields of ≈70% were obtained at 353K after 7 hours of reaction. Surface Sn species participate in the kinetically relevant reaction steps.

Keywords: ethyl lactate; dihydroxyacetone; ethanol; Lewis acid; sugars

1. Introduction

In recent years, the synthesis of alkyl esters of lactic acid (alkyl lactates) has attracted much attention because they can be obtained from renewable resources. They are currently produced from lactic acid and alcohols (methanol, ethanol, butanol) using mineral acids as catalysts, with the consequent technological and environmental hazard. Several works describe the synthesis by heterogeneous catalysis using Amberlyst 15, Dowex 50W and heteropolyacids, but the process is equilibrium-limited reaching conversions of just 35% [1,2,3].

Alkyl lactates are high boiling point liquids used as solvents and plasticizers for cellulose plastics and vinyl resins, among other many applications. They also take part in cosmetic and herbicidal formulations and are used as skin whitening products [4]. In particular, ethyl lactate (EL) is widely used as a green solvent to replace chlorinated hydrocarbons [5]. It presents environmental, technological and economic advantages for many industrial applications. It is biodegradable, harmless, recyclable and non-corrosive

[6]. In addition to the above-described uses of alkyl lactates, EL is used in pharmaceutical formulations for the treatment of acne and seborrhea [4].

Lately, many works report the synthesis of alkyl esters of lactic acid from triose sugars such as dihydroxyacetone (DHA) and short chain alcohols using acid catalysts. This procedure presents the advantage that the extent of reaction is not limited by the equilibrium. Furthermore, DHA can be obtained in a biorefinery by glycerol oxidation [7] or by cellulose hydrolysis followed by isomerization and retro-aldol reactions [8]. The pioneering works describe the use of alcohol solutions of tin chlorides as homogeneous catalysts [9], zeolites [10,11,12,13] and mixed oxides [14]. More recently, many works have been devoted to study the performance of Sn-containing solids such as mesoporous materials (MCM-41 [8,15], SBA-15 [16]), clays [17] and zeolites (MFI [18], BEA [19,20,21,22,23]) during this synthesis. Some authors claim that Brønsted acid sites [11,17] or a combination of mild Brønsted and Lewis acid sites [8,15,19] promote the alkyl lactate formation from DHA. In contrast, other researchers postulate that the Lewis acid sites of Sn-substituted BEA zeolites are responsible for the catalytic activity [20]. In any case, the use of Sn-modified materials such as MCM-41 or BEA zeolite for the production of alkyl lactates may be limited not only by the cost and long synthesis time of these solids but also by the large solid quantities needed for the scaling up of a commodity production.

Here, we present our investigations on the synthesis of ethyl lactate from DHA and ethanol on inexpensive and easily scalable alumina-supported Sn catalysts prepared by impregnation. For this purpose, a series of tin containing catalysts coded as ZSnAl (Z =1.4, 4.2 and 7.6wt.% Sn) was prepared. These materials were characterized by several techniques in order to determine their structural, textural, and optical properties, with special emphasis on the knowledge of acid site nature and number. The role of the tin loading on the generation of surface acid sites was investigated as well as the participation of Sn species in the kinetically relevant reaction steps. We found that the ZSnAl catalysts convert DHA at mild conditions through a series of reaction steps leading to formation of ethyl lactate and other valuable oxygenates, Scheme 1; these materials present a catalytic performance comparable to those of other catalytic solids reported in the literature.

1. Experimental

2.1 Catalyst synthesis

Alumina-supported tin catalysts containing 1.4, 4.2 and 7.6 wt.% Sn were prepared by incipient wetness impregnation of commercial γ-Al_2O_3 Cyanamid Ketjen CK 300 with aqueous solutions of $SnCl_4.5H_2O$ (Aldrich, 98%). Catalysts were denoted as ZSnAl, where Z is the Sn content expressed in wt.%. The ZSnAl precursors were thermally treated overnight (18 h) in flowing air at 573K. Another set of catalysts was prepared using aqueous solutions of anhydrous $SnCl_2$ (Riedel-de Haën, 98%) and precursor calcination in air at 573K and 773K; these catalysts were coded as 4.8SnAl-D-573 and 4.0SnAl-D-773, respectively.

Pure SnO_2 was prepared by precipitation of $SnCl_4.5H_2O$ with urea at 363K, according to the procedure of Acarbas et al [24]. After washing and drying at 363K, the precipitate was calcined at 573K in flowing air for 3h.

The commercial γ-Al_2O_3 was treated at 773K in flowing air for 3h to remove adsorbed water before the impregnation procedures.

2.2 Catalyst characterization.

BET surface areas (*SA*) were measured by N_2 physisorption at 77K using an

Autosorb Quantachrome 1-C sorptometer. After calcination, the chemical content of Sn and of residual Cl was analyzed by inductively coupled plasma (ICP-OES). The catalyst structural properties were determined by X-Ray Diffraction (XRD) between 20 and 80° using a Shimadzu XD-D1 instrument with nickel filtered Cu Kα radiations. Crystallite size was calculated employing the Debye-Scherrer equation: $L = 0.9\lambda/\beta \cos \theta$, where L is the crystallite size, λ is the wavelength of the used radiation, β is the full width at half-maximum and θ is the Bragg diffraction angle.

UV-vis-DRS experiments were carried out using a Perkin Elmer Lambda 40 spectrophotometer equipped with a diffuse reflectance chamber and integrating sphere (Labsphere RSA-PE-20) coated internally with polytetrafluoroethylene (PTFE). Prior to each experiment, samples were compacted in a sample holder to obtain a sample thickness of ≈2 mm. Spectra were recorded at room temperature in reflectance mode (R) between 200 and 800 nm and converted to the Kubelka-Munk function: $F(R_\infty) = (1 - R_\infty)^2/2\,R_\infty = K\,C$, where K is a constant including the sample scattering coefficient and absorptivity, and C is the analyte concentration [25]. The material used as reference was PTFE.

Total acid site number (n_a, μmol/g) and acid site density (N_a, μmol/m^2) were determined by TPD of NH_3. Samples were thermally treated in He at the corresponding calcination temperature and then exposed to a 1.01% NH_3/He flow at 373 K during 30 min to enable surface saturation. Weakly adsorbed NH_3 was removed by flushing with He. The temperature was then increased at a rate of 10 K/min from 373K to 593K and kept constant for 1h. NH_3 concentration in the reactor effluent was monitored by a mass spectrometer (MS) detector in a Baltzers Omnistar unit.

The chemical nature of the acid sites present on the catalyst surface was determined by Infrared Spectroscopy (IR) of pyridine adsorbed at room temperature and evacuated at increasing temperatures. Experiments were carried out using a Shimadzu FTIR Prestige-21 spectrophotometer. An inverted T-shaped cell containing the sample wafer and fitted with CaF_2 windows was used. In a typical experiment, the sample wafer was evacuated at 573K and then cooled down to room temperature to take the catalyst spectrum. After that, the sample was exposed to 0.12 kPa of pyridine at room temperature and then evacuated consecutively at 298, 373, 423 and 473K. The resulting spectrum at each evacuation temperature was recorded at room temperature. Spectra of the adsorbed species were obtained by subtracting the catalyst spectrum. The absorbance scales of the absorbed species spectra were normalized using the wafer density ($\rho = W/S$; W is the wafer weight in grams and S the wafer area in cm^2). An indication of the number of Lewis acid sites (n_L, μmol/g) was determined based on the Lambert-Beer equation,

$$n_L = \frac{LA}{\varepsilon_L \, \rho}$$

where LA (Lewis area in cm^{-1}) stands for the integrated absorption of the band at $1450 cm^{-1}$ corresponding to pyridine coordinated to Lewis acid sites, and ε_L is the molar extinction coefficient taken as 0.64 cm/μmol [26,27].

2.3 Catalytic testing

The liquid-phase reaction of dihydroxyacetone, DHA (Aldrich, 97%) with ethanol (Merck, 99.8%) was carried out at 353K and at an autogenous pressure of 250 kPa in a batch PARR reactor. In a typical experiment, a solution of DHA in ethanol with ethanol/DHA=43 (molar ratio) was loaded in the reactor and a catalyst/DHA weight ratio of 43% was used. Catalysts were thermally treated ex-situ in air flow at the corresponding calcination temperature to remove adsorbed water. After introducing the reactant mixture the reactor was sealed and flushed with N_2 and then the mixture was heated up to the reaction temperature under stirring (400 rpm). Then, the catalyst as ground powder was added to the reaction mixture to start the reaction. Inter- and intra-particle diffusional limitations were verified to be negligible. Quantification of reaction products was carried out after proper product identification using a Thermo Scientific Trace 1300 gas chromatograph (GC) with a Thermo Scientific TR-5MS capillary column coupled to a Thermo Scientific ISQ QD MS unit. Main reaction products were glyceraldehyde (GLA), pyruvic aldehyde (PA), ethyl lactate (EL), pyruvic aldehyde hemiacetal (PAHA) and pyruvic aldehyde diethyl acetal (PADA). Minor products include glyceraldehyde diethyl acetal. Solutions containing weighted amounts of the different reactants and products and the standard (n-octanol, BDH, 99%) were injected in the GC; the compound concentration was varied in each solution. Molar response factors relative to the standard were calculated using the GC peak area of each compound and the corresponding molecular weight. All reagents were analytical grade.

Yields (Y_i, mol of product i/mol of DHA at t=0) were calculated as $Y_i = S_i X_{DHA}$, where X_{DHA} is the conversion of DHA and S_i is the selectivity of product i (S_i, mol of product i/mol of DHA reacted). Selectivity was calculated as $S_i = C_i/\Sigma C_i$, where C_i is the concentration of product i.

The initial DHA conversion rate (r^0_{DHA}, mmol/h g cat) was calculated from the initial slope of the X_{DHA} vs. time curve after multiplication by n^0_{DHA}/W, where n^0_{DHA} is the number of moles of dihydroxyacetone in the reactor at t=0 and W the catalyst load. Initial turnover rate (TOR^0, min^{-1}) is defined as the moles of DHA converted per minute and per mole of acid site measured by NH_3 TPD. Ethyl lactate productivity (P_{EL}) was calculated as grams of EL produced per kilogram of catalyst and per hour at the end of the 7h-run.

3. Results and discussion

3.1 Catalyst characterization

The ZSnAl catalysts were prepared by incipient wetness impregnation of commercial γ-Al_2O_3 with $SnCl_4.5H_2O$ followed by calcination. They were analyzed by several techniques in order to study their chemical, structural, textural and acid properties. Results are summarized in Table 1.

In all the alumina-supported Sn catalysts the chlorine content remaining after calcination in air was below 0.3 wt. % irrespective of the Sn loading and preparation procedure. Catalysts presented slightly lower *SA* values than Al_2O_3. This is probably due to pore blockage by tin species during preparation procedures.

The structural analysis by XRD, Figure 1, shows that regardless of the preparation conditions, no crystalline Sn species could be detected in spite of the wide Sn compositional range used. Thus, Sn species are well dispersed on the alumina surface forming small domains not detectable by XRD even at loadings close to 8wt. %. This is striking considering that calculations of the SnO_2 monolayer coverage fraction indicate that 25% of the alumina surface would be covered by SnO_2 in sample 7.6SnAl.

Alumina is a solid with a defect spinel structure in which the Al^{3+} cations occupy tetrahedral (Td) and octahedral (Oh) positions so that about 30% of the cations are in tetrahedral coordination (Al_{Oh}/Al_{Td} = 2.36) [28]. Thus, in the ZSnAl samples, the possible presence of Sn species with different coordination and degree of interaction with the alumina support was investigated by UV-vis-DRS. In Figure 2A the spectra of reference materials, a commercial γ-Al_2O_3 and a mechanical mixture of 7.8 wt.% SnO_2-alumina, were plotted as Kubelka-Munk function vs. wavelength. The latter shows signals similar to those reported in the literature for bulk SnO_2 with a band at ≈220 nm and a broad double band at about 275-300 nm assigned to hexacoordinated polymeric

Sn-O-Sn type of species [19,29,30]. On the other hand, alumina does not show any relevant signal.

The spectra of the ZSnAl samples plotted in Figure 2A present a main band at ≈205 nm and very weak bands at ≈265 and ≈298nm (inset in Figure 2A) which are typical features of SnO_2 nanoparticles [31,32]. For semiconducting nanoparticles, the UV-vis-DRS technique is very sensitive not only to cation coordination but to SnO_2 particle size since the absorption edge is expected to shift to a higher energy value when the particle size decreases [31,33]. Thus, the blue-shift (lower wavelength) of the band at 205nm respect to the spectrum of bulk SnO_2 (275-300 nm) is attributed to dispersed Sn^{4+} species forming amorphous domains in ZSnAl samples that strongly interact with the alumina support. In these species, the Sn^{4+} cations would be probably surrounded by less oxygen anions than in the octahedral coordination [34].

In order to investigate in a comparative fashion the particle size of Sn species in ZSnAl samples with different Sn loadings, their band gap energies were studied by UV-vis-DRS following the procedure of Roy et al. [35]. The Kubelka-Munk function $F(R_\infty)$ was used to determine the band gap energy (Eg). Figure 2B shows the plots of $[F(R_\infty) \times (h\nu)]^2$ vs $h\nu$. The Eg values were obtained by extrapolation of the linear part of the plots to the *X*-axis (straight lines in Figure 2B) and the results are summarized in Table 1. The Eg of bulk SnO_2 (3.52 eV) was similar to values reported before (3.65-3.95 eV) for nano-sized oxides [31,33]. In fact, the crystallite size of our home-made SnO_2 calcined at 573K was 4nm (calculated from the XRD pattern of Figure 1), a value similar to that reported by Pang et al [31] for an oxide obtained at 673K.

The calculated Eg values (4.8-5.1 eV) for the Sn-containing samples (Table 1) are in agreement with the determinations of Dvininov et al [34] for SnO_2 particles prepared by wet impregnation of $SnCl_4.5H_2O$ on a Mg-Al-layered double hydroxide followed by hydrolysis and calcination. As stated above, the larger the SnO_2 particle size, the lower the energy. Thus, for the ZSnAl samples, the shift of Eg to higher values compared to bulk SnO_2 indicates smaller SnO_2 particles than in the reference sample. Furthermore, the gradual decrease of the Eg values (Table 1) as Z increases from 1.4 to 7.6 wt. % Sn, results in a concomitant increase of the SnO_2 cluster size. Thus, agglomeration of SnO_2 species occurs in ZSnAl samples with higher Sn loadings giving rise to bigger particles. In Figure 2A the lower signal intensity of sample 7.6SnAl compared to 4.2SnAl is in line with this finding.

The surface acid properties of the ZSnAl samples were investigated by combining NH_3 TPD and FTIR of pyridine. The desorption profiles of Figure 3 present similar desorption features as Z increases. A broad desorption peak centered at 580-590K indicates the presence of acid species that adsorb NH_3 with different binding energies. The desorption temperature range and the n_a values of the ZSnAl samples are much higher than those of pure γ-Al_2O_3. These results suggest that in the former, surface Sn species are responsible for the generation of new and stronger acid sites compared to those of γ-Al_2O_3. Furthermore, the number of acid sites n_a (measured as the area under the TPD curve, Table 1) increases linearly with Z as shown in open circles in Figure 4.

The chemical nature of the surface acid sites present on ZSnAl and γ-Al_2O_3 catalysts was studied by FTIR of pyridine preadsorbed at room temperature and evacuated at increasing temperatures. Figure 5A and 5B present the spectra of the ν_{CCN} and ν_{OH} region, respectively, after evacuation at 423K. In the spectra of the ν_{CCN} region, Figure 5A, the Lewis acid character of the ZSnAl samples was confirmed by the bands at 1450 and 1618cm^{-1} assigned to pyridine coordinated on the oxide cations [36]. The shoulder on the high frequency side of both bands probably indicates the presence of Sn^{4+} and Al^{3+} cations in different chemical environments, as discussed above. The acid strength of the Lewis centers generated on the ZSnAl samples by Sn doping seems to depend on the Sn loading, so that an acid strength increase can be envisaged by the shift toward higher frequencies of the band at 1450 cm^{-1} as Z increases [37].

The spectra of Figure 5A do not show any band at 1640 and 1550 cm^{-1} which is an indication of the absence of Brønsted acid sites strong enough to protonate pyridine. However, the bands in the ν_{OH} region of the spectra, Figure 5B, suggest the presence of OH species weakly interacting with pyridine at 423K. In fact, the broad bands in the ν_{OH} region corresponding to the ZSnAl samples before pyridine adsorption, Figure 5C, confirm the presence of isolated surface OH groups with different coordination numbers, i.e., bridging and multi-centered OH (3750-3650 cm^{-1}) [38]. The OH species remain on the surface after calcination of the ZSnAl oxides owing to the low treatment temperature used in the preparation procedures (573K). These OH bands are more evident on γ-Al_2O_3 and decrease with increasing the Sn loading. Therefore, sample 7.6SnAl in Figure 5C presents mainly one broad band centered at 3567 cm^{-1} attributed to H-bonded OH groups. In agreement with that, the number of OH species interacting with pyridine decreases as Z increases, as indicated by the intensity of the negative peaks at 3800-3600cm^{-1} shown in Figure 5B.

In an attempt to use in a quantitative fashion the FTIR results of Figure 5A, the number of Lewis acid sites (n_L) was calculated for the ZSnAl samples and plotted as closed circles in Figure 4. A good agreement was found between n_L and the n_a values determined by TPD of NH_3.

3.2 Effect of preparation conditions

The influence of the preparation conditions on the physicochemical properties of the alumina-supported Sn catalysts was studied. At similar Sn loadings, no effect of the Sn oxidation state (Sn^{4+} or Sn^{2+}) in the impregnating salt solution was found; when $SnCl_2$ was used (sample 4.8SnAl-D-573), the *SA* value, the structural, optical and acid properties were similar to those of sample 4.2SnAl prepared from $SnCl_4.5H_2O$ (Table 1 and Figures 1, 3, 4 and 5A). Likewise, no effect was observed on the residual chlorine content. Thus, the use of $SnCl_4.5H_2O$ was preferred due to its higher solubility in water and easier handling.

The effect of the calcination temperature was investigated with two samples prepared from $SnCl_2$ (samples 4.8SnAl-D-573 and 4.0SnAl-D-773, Table 1). The alumina support was stabilized at 773K before impregnation and therefore, the slight decrease of the *SA* upon increasing the calcination temperature from 573K to 773K is likely due to agglomeration of the Sn phase and pore blockage rather than to a collapse of the porous structure of alumina. This SnO_2 particle size increase is not detected by XRD in Figure 1 but is evident in the Eg values of Table 1; in the sample calcined at higher temperature the Eg shifted to lower values reflecting the presence of larger SnO_2 domains. In addition, the n_a value also decreased as a consequence of the particle agglomeration (open down triangle in Figure 4).

3.3 Sn-catalyzed DHA conversion reactions under homogeneous and heterogeneous conditions

Preliminary blank tests were carried with DHA and ethanol at 353K without any catalyst. Thermal reactions were ruled out since no measurable conversion was found after 7h under those conditions.

The conversion of DHA with ethanol was studied under homogeneous catalysis conditions using a DHA/Sn≈74 (molar ratio) and ethanol solutions of $SnCl_4.5H_2O$ or $SnCl_2$ (entries 7 and 8 in Table 2). In both cases, total conversion was attained at 3h. In both tests, after 3h the ethyl lactate (EL) yield increased at the expense of that of pyruvic aldehyde (PA) reaching values of 78-83% at the end of the 7h-run. Tin chlorides have been shown by Hayashi et al [9] to be excellent catalysts for conversion of trioses (DHA and GLA) into alkyl lactates with a superior performance than other metal halides. They assigned this unique property of tin chlorides to the way they interact with pyruvic aldehyde (PA); rather than being just a Lewis acid center, Sn in $SnCl_x$ species might strongly coordinate to the substrate to form a specific intermediate that would give rise to alkyl lactate formation by a 1,2-hydride shift mechanism. In agreement with the results of these researchers, the comparison of the two chlorides after 7h of reaction, Table 2, shows that slightly higher EL yields were obtained using $SnCl_4.5H_2O$.

The catalytic performance of our Sn-promoted solid catalysts prepared by different procedures (Table 2, entries 2, 4 and 5) was compared under similar reaction conditions (353K and DHA/Sn≈74) with the homogeneously catalyzed tests (entries 7 and 8). After 7h of reaction, the EL yields of the alumina-supported Sn samples calcined at 573K and prepared from $SnCl_4.5H_2O$ (entry 2) and $SnCl_2$ (entry 4) were lower than in the homogeneous tests and not much dependent on the preparation technique. But the X_{DHA} values of the heterogeneous tests at the end of the 7h-run were close to those obtained by homogeneous catalysis in 3h. Although the time difference is not large, this result indicates that the SnO_2 particles present on the solids with similar Sn loadings are less efficient than the $SnCl_x$ solutions to convert DHA regardless of the tin oxidation state in the impregnating salt. On the other hand, sample 4.0SnAl-D-773 (entry 5) that because of calcination at 773K contains larger SnO_2 particles and a lower number of acid sites (n_a), gave the lowest X_{DHA} and ethyl lactate productivity (P_{EL}, g EL/kg cat h) after 7h.

The P_{EL} values (≈200 g EL/kg cat h) obtained at 353K on our alumina-supported Sn samples with ≈4wt.% Sn and calcined at 573K can be more than twofold enhanced (528 g EL/kg cat h) by increasing the reaction temperature to 373K and the Sn loading to 7.6wt.% (Table 2, entry 9). Our P_{EL} values compare favorably with those of other solid catalysts tested at higher reaction temperatures (363-433K), such as zeolites [10,11], Zr-Ti mixed oxides [14], Zn-MCM-41 [39] and Sn-MCM41[8,15] but they are lower than those obtained on Sn-dealuminated BEA zeolites tested at 363K [19,20].

The heterogeneous nature of the DHA and ethanol conversion on Sn-promoted alumina catalysts was confirmed by removing the solid catalyst after X_{DHA}≈100% was reached at 353K and then adding a fresh DHA load. The reaction was continued for 4 more hours at 353K but no conversion was observed.

3.4 Reaction pathways and active sites on ZSnAl catalysts

The ZSnAl samples of Table 1 prepared by impregnation of alumina with aqueous solutions of $SnCl_4.5H_2O$ were tested in the conversion of DHA and ethanol to ethyl lactate. Figure 6 shows the time evolution of the DHA conversion (X_{DHA}) and of the major product yields on the ZSnAl catalysts containing different Sn loadings. Main products were ethyl lactate (EL), pyruvic aldehyde (PA), pyruvic aldehyde diethyl acetal (PADA) and pyruvic aldehyde hemiacetal (PAHA). The shape of the curves clearly indicates that PA and PAHA are reaction intermediates whereas PADA and EL are final products as postulated in Scheme 1. Thus, longer reaction times than those of Figure 6 would increase the final EL yield because of the additional PA transformation into EL.

The reaction steps conducting to EL and other products are depicted in Scheme 1. The reaction starts by DHA isomerization to glyceraldehyde (GLA) [40], step 1.

Formation of GLA cannot be avoided but under our reaction conditions the equilibrium of step 1 is expected to be shifted toward DHA [13,41]. Since both trioses give similar product distribution when react with an alcohol [10,11], in our calculations the overall conversion of both trioses (coded as X_{DHA}) was quantified. The pathway to reaction products bears the initial triose (DHA and GLA) dehydration to PA, step 2.

From PA the reaction pathway might proceed by re-arrangement with incorporation of an alcohol molecule toward the desired ethyl lactate product, step 3, or toward PAHA (step 4) and PADA (step 5) by addition of an alcohol molecule in each of these reaction steps. Step 6 is the isomerization of PAHA to EL. The fact that in Figure 6A the PAHA curve goes above that of PA at short reaction times suggests that step 5 is reversible. In agreement with that, West et al. have observed a decrease in the PADA yield on zeolites but at reaction times much longer than the time frame of our experiments [11].

In previous works, the role of Brønsted and Lewis acid sites on alkyl lactate and other oxygenate formation from DHA and alcohols has been discussed [10,11,12]. It is generally accepted that PA formation is promoted by mild Brønsted acid sites but some authors claim the participation of Lewis acid sites [8,13]. The subsequent pathways toward formation of EL or PADA involve sites with different acid nature; the former occurs on Lewis acid sites whereas the latter takes place on Brønsted acid sites. Therefore, the presence of strong Brønsted acid sites should be avoided, because in the overall process they convert DHA into PADA. Thus, weakly acidic Brønsted sites and Lewis acid sites seems to be a suitable combination to promote EL formation. The role of the Lewis sites has been shown to be the 1,2-hydride shift during re-arrangement of PA, step 3, or PAHA, step 6 [15,23].

The Lewis acid nature of the surface species generated on alumina by Sn doping was verified by the FTIR experiments of Figure 5. Since alumina presented low activity for the reaction (Table 2, entry 6), the better catalytic performance of the Sn-containing oxides must be attributed to Sn species. Thus, based on the mechanism reported by Hayashi et al [9] for the homogenous synthesis of alkyl lactates from trioses using Sn chlorides, we postulate here in Scheme 2 the possible surface pathway for step 3 on the ZSnAl oxides, i.e., the Sn-mediated conversion of PA into EL. PA is activated on tin species forming a cyclic intermediate in which Sn is coordinated to both C=O groups of PA. On the other hand, ethyl alcohol can be dissociatively adsorbed through the O-H bond on Sn-O or Al-O pair sites giving rise to a surface ethoxide intermediate and a surface hydrogen atom. The next step is the nucleophilic addition of the ethoxide to the terminal carbonyl function of PA, followed by an intramolecular rearrangement with a 1,2-hydride shift and formation of an anionic cyclic intermediate. Then, the latter interacts with the adjacently adsorbed hydrogen atom to yield ethyl lactate.

The other possible surface pathway conducting to EL on ZSnAl samples, i.e., the isomerization of PAHA, step 6 of Scheme 1, is also depicted in Scheme 2. It involves a bidentate PAHA coordination on a Sn atom and the O-H bond breaking on a surface acid-base pair site. The following step is the formation of an intermediate similar to that of the pathway from PA, and intramolecular rearrangement with a shift of the hydride.

Notwithstanding we have included step 3 in the reaction Scheme 1, a preliminary kinetic modeling (not shown here) indicated a better fit of the results of Figure 6 when the rate equations were regressed setting k_3 (the kinetic constant of step 3) to zero. Therefore, formation of EL mainly proceeds through the PAHA intermediate in agreement with the results of Li et al. on Sn-MCM-41 [15] and of van der Graaff et al. on Sn-BEA [23]. Thus, the thickness of the arrow lines in Scheme 2 indicates the relative importance of the two mechanisms toward EL emphasizing that most of the EL product arises from PAHA and to a lesser extent directly from PA.

Formation of PADA among the reaction products suggests that the isolated OH groups present on the surface of the Sn-promoted oxides, as shown in Figure 5C, might behave as weak Brønsted acid sites that participate in steps 4 and 5 of Scheme 1. In fact, the sample prepared from $SnCl_2$ and calcined at 573K (4.8SnAl-D-573), that shows a higher degree of surface hydroxylation than that treated at 773K (4.0SnAl-D-773), gives a lower EL/PADA ratio when compared at 85% DHA conversion (Table 2). In Figure 5C a gradual decrease of the surface hydroxylation as Z increases can be observed. This suggests that upon impregnation, Sn species displace the OH groups from the surface. In line with that, on the ZSnAl catalysts the yield to PADA at 85% conversion decreases in the order of 9.4, 8.8, 6.2% as Z increases from 1.4, 4.2 to 7.6wt.% Sn.

Another explanation for PADA formation is the in situ generation of weak Brønsted acid sites during reaction due to water formation in step 2. However, the amount of these new OH species should be low since ethanol competes favorably with water for the adsorption sites and probably displaces it from the surface [42].

Scheme 3 shows the possible formation of PADA by esterification of PAHA with ethanol on weak Brønsted sites.

3.5 Effect of the Sn content and acid properties on the catalytic performance of ZSnAl catalysts

As we stated above, alumina was poorly active under our reaction conditions. Although alumina is a Lewis acid, it seems that the Al^{3+} cations are not acidic enough to transform DHA to a significant extent. The main product was PAHA owing to the low DHA conversion and in agreement with the weak acid properties probed in Figure 3. On the other hand, our alumina-supported Sn catalysts are Lewis acid solids in spite of the fact that the alumina surface is partially hydroxylated after calcination at 573K. In fact, it has been shown that highly hydroxylated alumina surfaces retain their Lewis acid character even in the presence of liquid water [42,43]. Thus, we assume that the measured number of acid sites (n_a) essentially corresponds to titration of Lewis acid centers provided by Al^{3+} and Sn^{4+} cations in different coordination numbers, as suggested by the results of Figure 4.

Figure 6 shows that both, the final DHA conversion and EL yield reached by the ZSnAl samples increase with the Sn loading. The higher number of acid sites (n_a, Figure 4) and the enhanced Lewis acid strength (Figure 5A) as Z increases explain the improved EL yields of Figure 6. It seems that the bimolecular nature of the reactions involved in DHA conversion requires not only a high concentration of Sn species available for reaction but also the close proximity of those species in order to allow the vicinal chemisorption of the different reaction intermediates.

To elucidate the participation of Sn species in the promotion of the reaction steps involved in the conversion of DHA with ethanol, the results obtained with the ZSnAl samples containing 1.4, 4.2 and 7.6 wt. % Sn were further investigated. From the initial slopes of the X_{DHA} vs time curves of Figure 6 the initial DHA conversion rates (r^0_{DHA}, mmol/hg) were calculated and the results are presented in Figure 7 (open symbols) as a function of n_a; commercial alumina and the samples prepared from $SnCl_2$ (4.8SnAl-D-573 and 4.0SnAl-D-773) were also included. The linear correlation suggests that Lewis acid sites are involved in the kinetically relevant steps of the DHA conversion. The initial turnover rate (TOR^0, min^{-1}) values of Table 2 are also plotted in Figure 7 (closed symbols). Similar TOR^0 values (≈6 min^{-1}) were obtained for the Sn-promoted samples regardless of the Sn loading or preparation procedure, which more than triple that of alumina (1.7 min^{-1}). This clearly confirms that highly dispersed Sn^{4+} species with

Lewis acid properties are responsible for most of the catalytic activity of the Sn-containing samples.

4. Conclusions

Alumina-supported Sn catalysts, which are easily prepared by impregnation, contain Lewis acid centers that efficiently promote conversion of trioses and ethanol into ethyl lactate at mild reaction conditions. Promotion with Sn generates more and stronger Lewis acid sites than those present on pure alumina. These sites participate in rate-limiting steps and therefore, the ethyl lactate yield is enhanced as the Sn loading increases.

Acknowledgements

Authors thank the Agencia Nacional de Promoción Científica y Tecnológica (ANPCyT), Argentina (grant PICT 1888/10), CONICET, Argentina (grant PIP 11220090100203/10) and Universidad Nacional del Litoral, Santa Fe, Argentina (grant CAID PI 64-103 /11) for financial support of this work.

References

---

[1] A. Corma, S. Iborra, A Velty, Chem. Rev. 107 (2007) 2411.

[2] A. Engin, H. Haluk, K. Gurkan, Green Chem. 5 (2003) 460.

[3] M.T. Sanz, R. Murga, S. Beltrán, J.L. Cabezas, J. Coca, Ind. Eng. Chem. Res. 41 (2002) 512.

[4] T.N.B. Kaimal, P. Vijayalakshmi, B. Ramalinga, A. A. Laxmi, US Patent N° 6342626, 2002.

[5] C.S.M. Pereira, V.M.T.M. Silva, A.E. Rodrigues, Green Chem. 13 (2011) 2658-

2671.

[6] S. Aparicio and R. Alcalde, J. Phys. Chem. B 113 (2009) 14257-14269.

[7] C.L. Bianchi, P. Canton, N. Dimitratos, F. Porta, L. Prati., Cat. Today, 102-103 (2005) 203-212.

[8] F. de Clippel, M. Dusselier, R. Van Rompaey, P. Vanelderen, J. Dijkmans, E. Makshina, L. Giebeler, S. Oswald, G.V. Baron, J. F. M. Denayer, P. P. Pescarmona, P.A. Jacobs, and B.F. Sels, J. Am. Chem. Soc. 134 (2012) 10089-10101.

[9] Y. Hayashi, Y. Sasaki, Chem. Comm. (2005) 2716-2718.

[10] P.P. Pescarmona, K.P.F. Janssen, C. Delaet, C. Stroobants, K. Houthoofd, A. Philippaerts, C. De Jonghe, J.S. Paul, P.A. Jacobs and B.F. Sels, Green Chem. 12 (2010) 1083-1089.

[11] R.M. West, M.S. Holm, S. Saravanamurugan, J. Xiong, Z. Beversdorf, E. Taarning, C. H. Christensen, J. Catal. 269 (2010) 122-130.

[12] K.P.F. Janssen, J.S. Paul, B.F. Sels, P.A. Jacobs, Stud. Surf. Sc. Catal. 70 (B) (2007) 1222-1227.

[13] P.Y. Dapsens, B.T. Kusema, C. Mondelli, J. Pérez-Ramírez, J. Molec. Catal. A: Chem. 388-389 (2014) 141-147.

[14] A.M. Mylin, S.I. Levytska, M.E. Sharanda, V.V. Brei, Catal. Comm. 47 (2014) 36-39.

[15] L. Li, C. Stroobants, K. Lin, P.A. Jacobs, B.F. Sels and P.P. Pescarmona, Green Chem. 13 (2011) 1175-1181.

[16] C. M. Osmundsen, M. S. Holm, S. D. and E. Taarning, Proc. R. Soc. A (2012) 1-17.

[17] J. Wang, Y. Masui, M. Onaka, Appl. Catal. B: Environm. 107 (2011) 135- 139.

[18] H.J. Cho, P. Dornath, and W. Fan, ACS Catal. 4 (2014) 2029-2037.

---

[19] J. Dijkmans, M. Dusselier, D. Gabriels, K. Houthoofd, P. C. M. M. Magusin, S. Huang, Y. Pontikes, M. Trekels, A. Vantomme, L. Giebeler, S. Oswald, and B. F. Sels, ACS Catal. 5 (2015) 928-940.

[20] C. Hammond, S. Conrad, and I. Hermans, Angew. Chem. Int. Ed., 51 (2012) 11736 -11739.

[21] E. Taarning, S. Saravanamurugan, M.S. Holm, J. Xiong, R.M. West and C.H. Christensen, ChemSusChem, 2 (2009) 625-627.

[22] S. Tolborg, A. Katerinopoulou, D.D. Falcone, I. Sádaba, C.M. Osmundsen, R.J. Davis, E. Taarning, P. Fristrup and M.S. Holm, J. Mater. Chem. A, 2 (2014) 20252-20262.

[23] W.N.P. van der Graaff, G. Li, B. Mezari, E.A. Pidko, and E.J.M. Hensen, ChemCatChem, 7 (7) (2015) 1152-1160.

[24] O. Acarbas¸ E. Suvaci, A. Dogan, Ceram. Intern. 33 (2007) 537-542.

[25] F. M. Mirabella, Modern techniques in applied molecular spectroscopy, first ed., Wiley-Interscience, New York, 1998.

[26] E. Selli, L. Forni, Microp. Mesop. Mat. 31 (1999) 129-140.

[27] M. Tamura, K. Shimizu, A. Satsuma, Appl. Catal. A: General 433-434 (2012) 135-145.

[28] V.K. Díez, C.R. Apesteguía, and J.I. Di Cosimo, J. Catal. 215 (2003) 220-233.

[29] N. K. Mal, A. V. Ramaswamy, J. Molec. Catal. A: Chem. 105 (1996) 149-158.

[30] R. Bermejo-Deval, R. Gounder, M. E. Davis, ACS Catal. 2 (2012) 2705-2713

[31] G. Pang, S. Chen, Y. Koltypin, A. Zaban, S. Feng, and A. Gedanken, Nano Lett.1(12) (2001) 723-726.

[32] H. Deng and J. M. Hossenlopp, J. Phys. Chem. B, 109 (2005) 66-73.

[33] M. Bhagwat, P. Shah, V. Ramaswamy, Mat. Lett. 57 (2003) 1604-1611.

[34] E. Dvininov, M. Ignat, P. Barvinschi, M.A. Smithers, E. Popovici, J. Hazard. Mat. 177 (2010) 150-158.

[35] S. Roy, K. Bakhmutsky, E. Mahmoud, R.F. Lobo and R. J. Gorte, ACS Catal. 3 (2013), 573-580.

[36] M. I. Zaki, M.A. Hasan, F.A. Al-Sagheer, L. Pasupulety, Colloids Surf. A: Phys. Eng. Asp. 190 (2001) 261-274.

[37] E.P. Parry, J. Catal. 2 (1963) 371-379.

[38] H. Knozinger, P. Ratnasamy, Catal. Rev. Sci. Eng. 17 (1978) 31-70.

[39] X. Collard, P. Louette, S. Fiorilli and C. Aprile, Phys. Chem. Chem. Phys. 17 (40) (2015) 26756-26765.

[40] V.A. Yaylayan, S. Harty-Majors, A.A. Ismail, Carbohyd. Res. 318 (1999) 20-25.

[41] R.S. Assary and L.A. Curtiss, J. Phys. Chem. A 115 (2011) 8754-8760.

[42] G. Busca, Catal. Today 226 (2014) 2-13.

[43] B. Kasprzyk-Hordern, Adv. Coll. Interf. Sc. 110 (2004) 19-48.

Caption to Figures

Figure 1: XRD patterns of ZSnAl catalysts (Z: wt.% Sn) prepared by different procedures, commercial γ-Al_2O_3 and home-made SnO_2.

Figure 2: UV-vis-DRS spectra of ZSnAl catalysts (Z: wt.% Sn) with different Sn loading. γ-Al_2O_3 and 7.8wt.% SnO_2-alumina included as references. (A) Kubelka-Munk function, $F(R_\infty)$, as a function of wavelength; (B) $[F(R_\infty) \times (h\nu)]^2$ vs $h\nu$ plot for band gap (Eg) energy determination.

Figure 3: TPD of NH_3 on ZSnAl catalysts (Z: wt.% Sn) prepared by different procedures. γ-Al_2O_3 included as reference.

Figure 4: Number of acid sites on ZSnAl catalysts prepared by different procedures as a function of the Sn loading. γ-Al_2O_3 included as reference [Open symbols: n_a values from TPD of NH_3, **Figure 3**; Closed symbols: Lewis sites (n_L) from FTIR of pyridine, **Figure 5A**].

Figure 5: FTIR of pyridine adsorbed at 298K and evacuated at 423K on the ZSnAl catalysts. γ-Al_2O_3 included as reference. (A) ν_{CCN} region; (B) ν_{OH} region; (C) ν_{OH} region before pyridine adsorption.

Figure 6: DHA conversion (X_{DHA}) and product yields as a function of reaction time on ZSnAl catalysts (A) Z=1.4wt.% Sn; (B) Z=4.2wt.% Sn; (C) Z=7.6wt.% Sn [Z: Sn loading; 353K; ethanol/DHA=43 (molar); 1g of catalyst].

Figure 7: Initial DHA conversion rate (r^0_{DHA}, open symbols) and turnover rate (TOR^0, closed symbols) as a function of the number of acid sites (n_a) of ZSnAl catalysts prepared by different procedures and γ-Al_2O_3 [353K; ethanol/DHA=43 (molar); 1g of catalyst].

Scheme 1: Reaction steps toward formation of ethyl lactate and other oxygenates from DHA and ethanol on ZSnAl catalysts.

Scheme 2: Postulated surface reaction mechanism on Sn sites for EL formation by steps 3 and 6 of **Scheme 1.**

Scheme 3: Postulated surface reaction mechanism on weak Brønsted acid sites for PADA formation by steps 4 and 5 of **Scheme 1.**

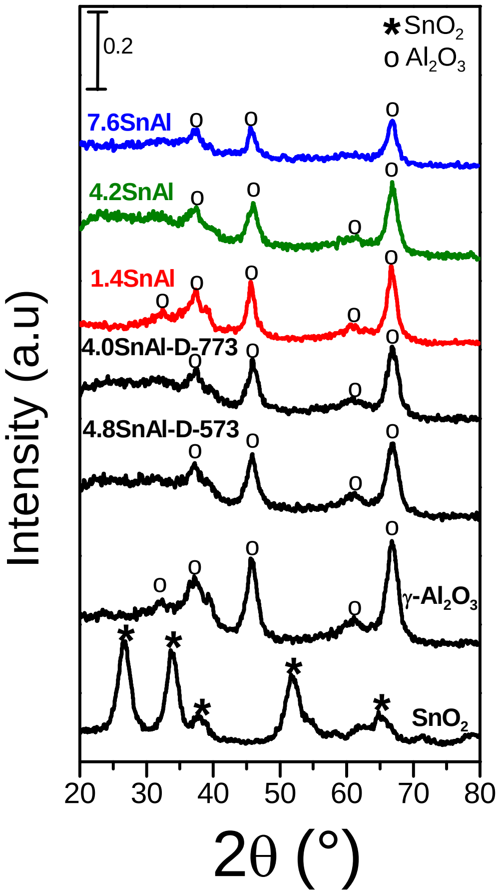

Figure 1: XRD patterns of ZSnAl catalysts (Z: wt.% Sn) prepared by different procedures, commercial γ-Al_2O_3 and home-made SnO_2.

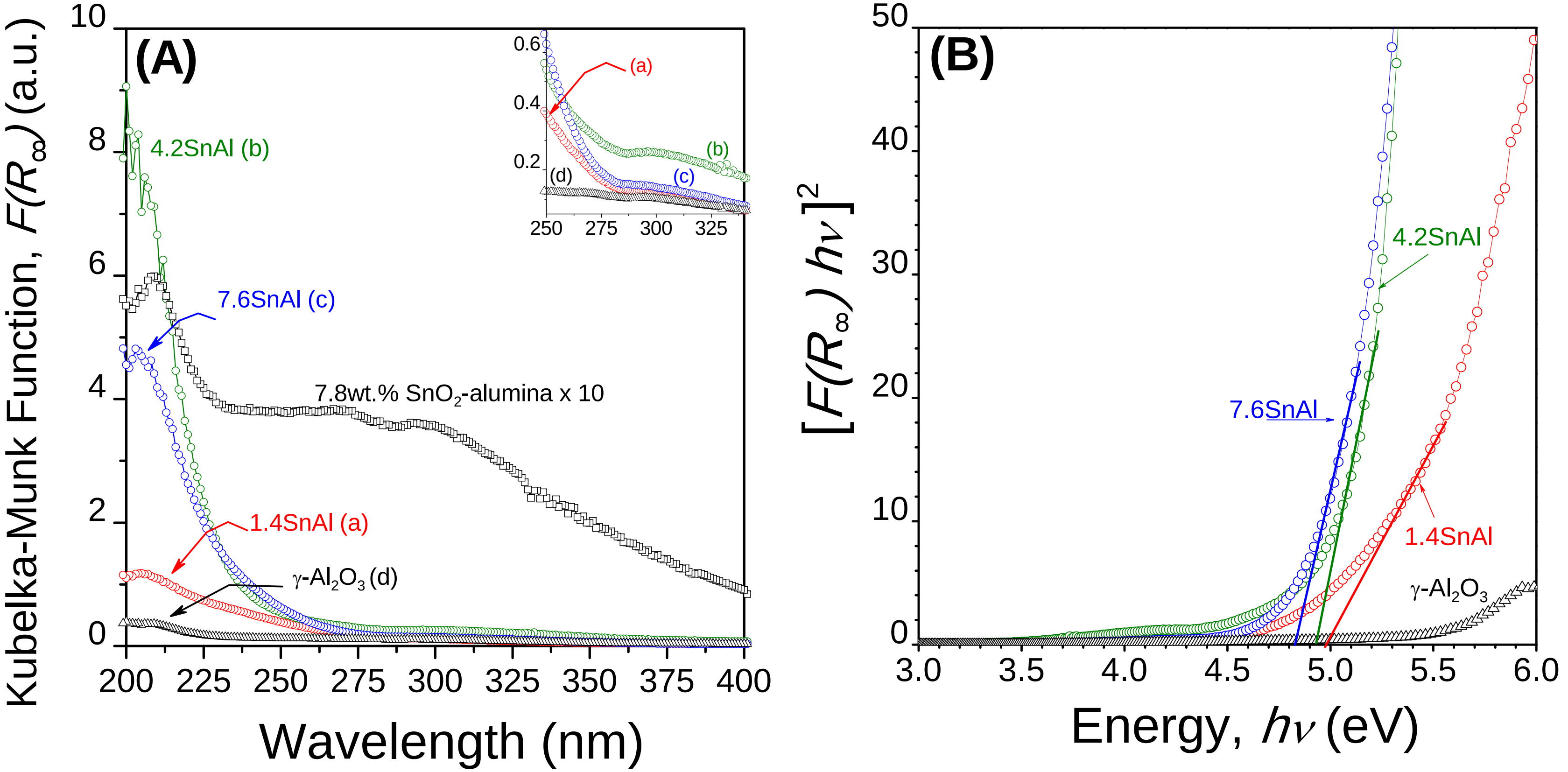

Figure 2: UV-vis-DRS spectra of ZSnAl catalysts (Z: wt.% Sn) with different Sn loading. γ-Al_2O_3 and 7.8wt.% SnO_2-alumina included as references. (A) Kubelka-Munk function, $F(R_\infty)$, as a function of wavelength; (B) $[F(R_\infty) \times (h\nu)]^2$ vs $h\nu$ plot for band gap (Eg) energy determination.

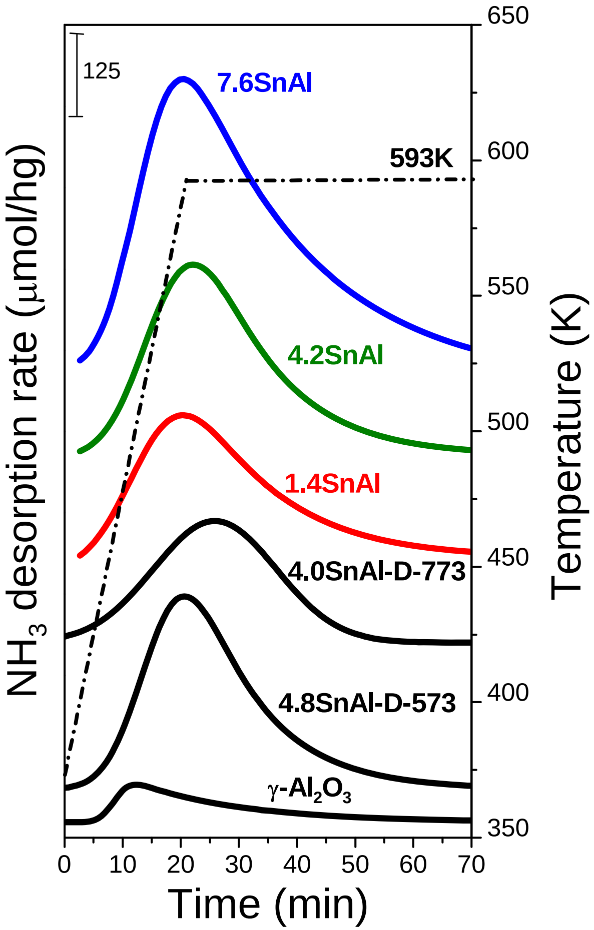

Figure 3: TPD of NH_3 on ZSnAl catalysts (Z: wt.% Sn) prepared by different procedures. γ-Al_2O_3 included as reference.

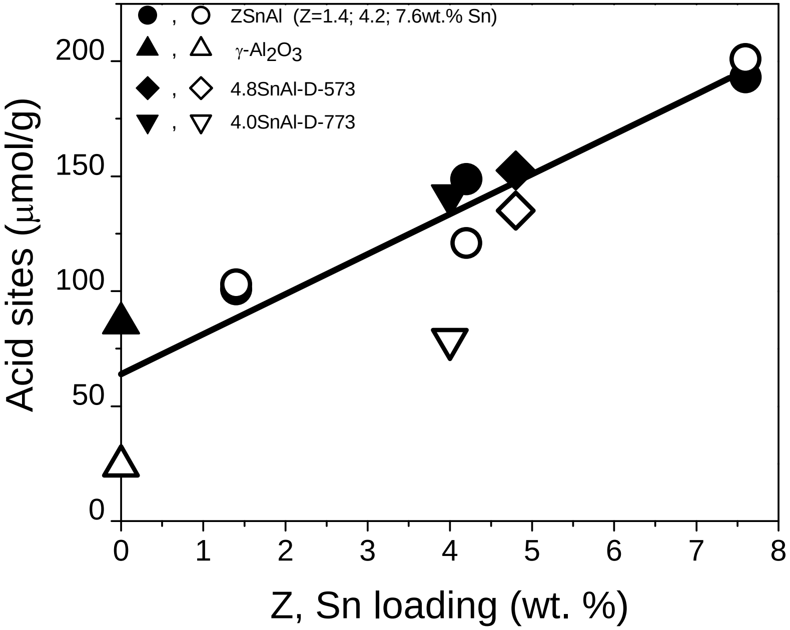

Figure 4: Number of acid sites on ZSnAl catalysts prepared by different procedures as a function of the Sn loading. γ-Al_2O_3 included as reference [Open symbols: n_a values from TPD of NH_3, Figure 3; Closed symbols: Lewis sites (n_L) from FTIR of pyridine, Figure 5A].

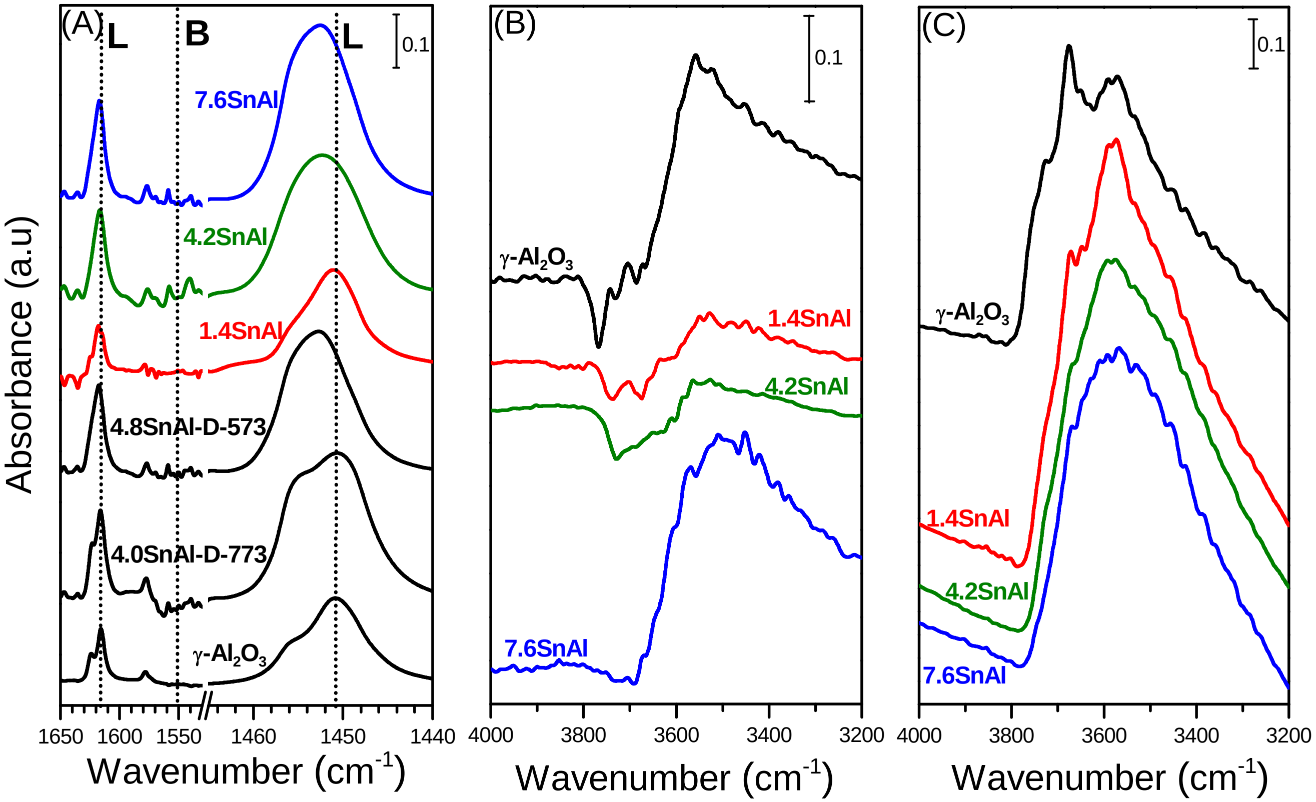

Figure 5: FTIR of pyridine adsorbed at 298K and evacuated at 423K on the ZSnAl catalysts. γ-Al_2O_3 included as reference. (A) ν_{CCN} region; (B) ν_{OH} region; (C) ν_{OH} region before pyridine adsorption.

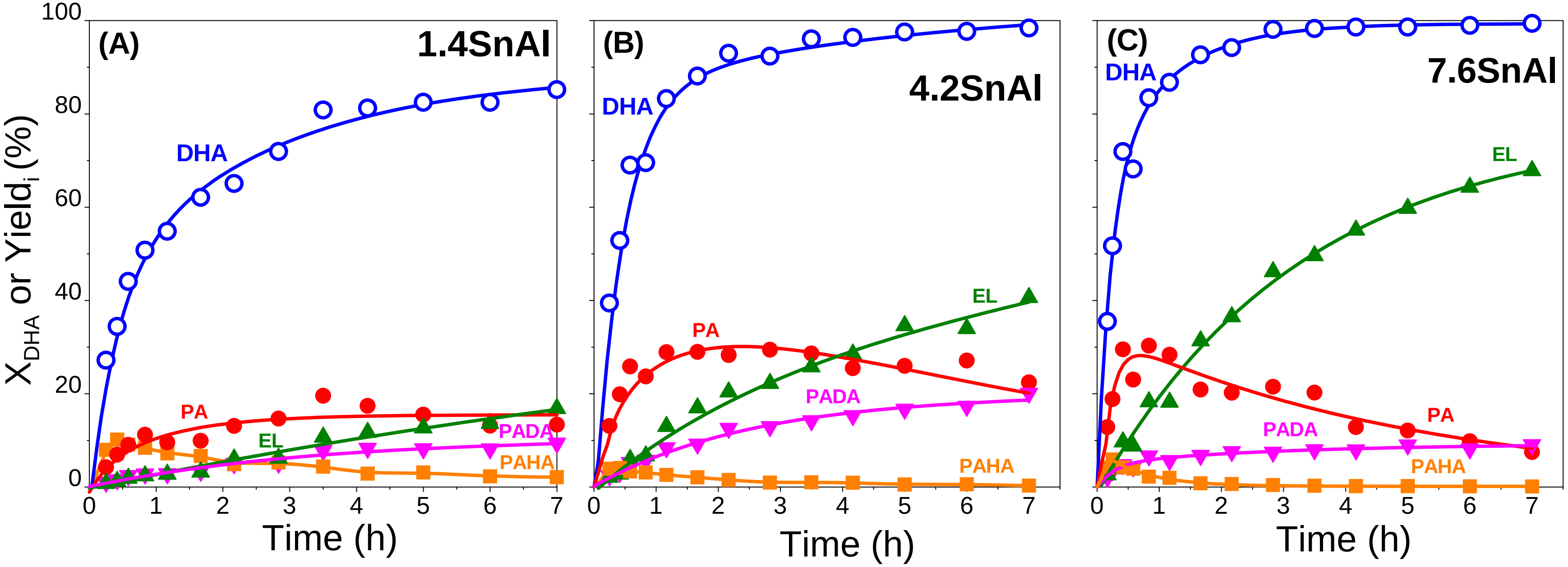

Figure 6: DHA conversion (X_{DHA}) and product yields as a function of reaction time on ZSnAl catalysts (A) Z=1.4wt.% Sn; (B) Z=4.2wt.% Sn; (C) Z=7.6wt.% Sn [Z: Sn loading; 353K; ethanol/DHA=43 (molar); 1g of catalyst].

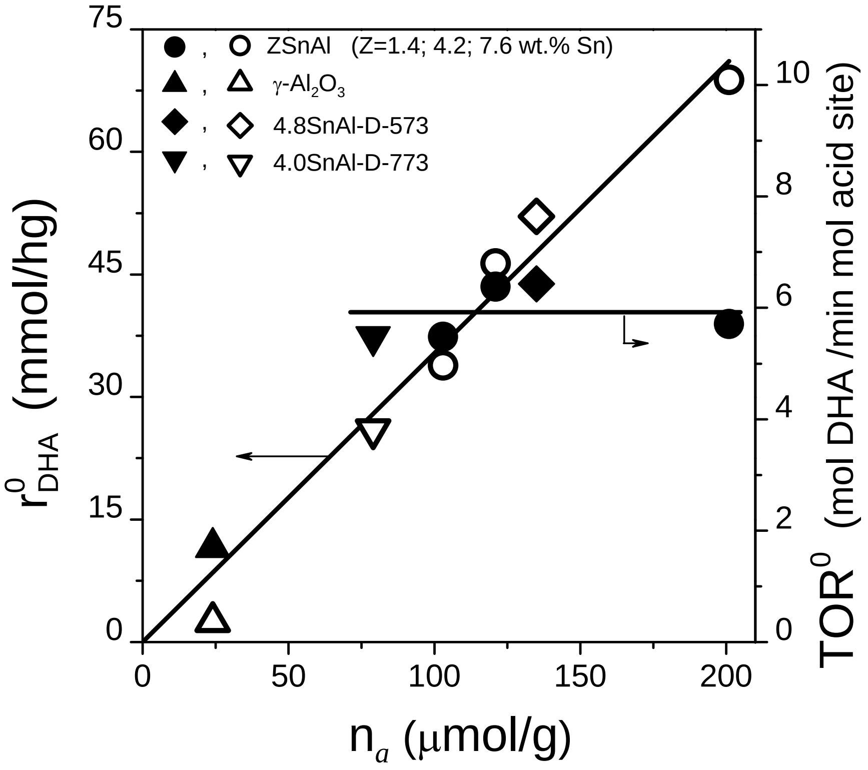

Figure 7: Initial DHA conversion rate (r^0_{DHA}, open symbols) and turnover rate (TOR^0, closed symbols) as a function of the number of acid sites (n_a) of ZSnAl catalysts prepared by different procedures and γ-Al_2O_3 [353K; ethanol/DHA=43 (molar); 1g of catalyst].

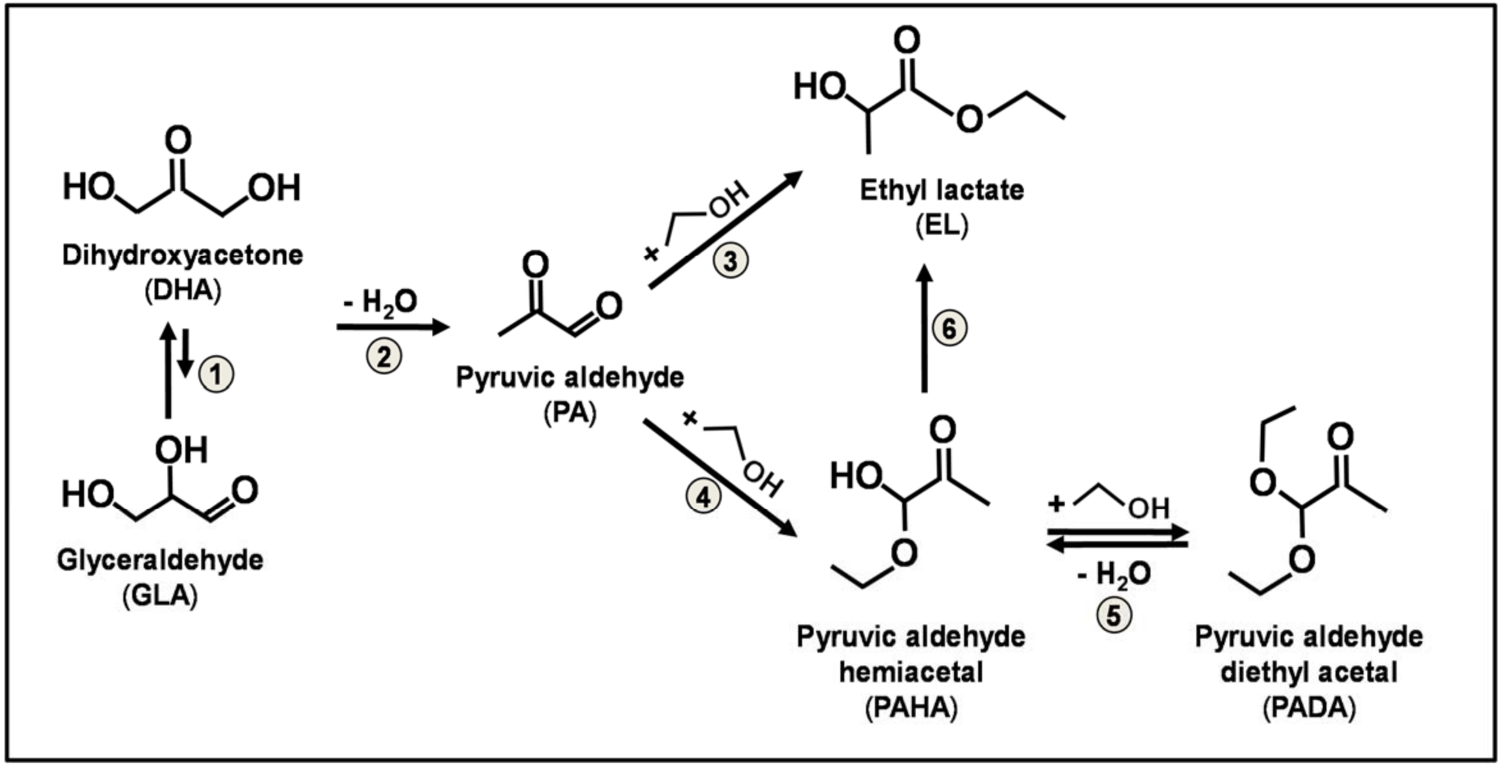

Scheme 1: Reaction steps toward formation of ethyl lactate and other oxygenates from DHA and ethanol on ZSnAl catalysts

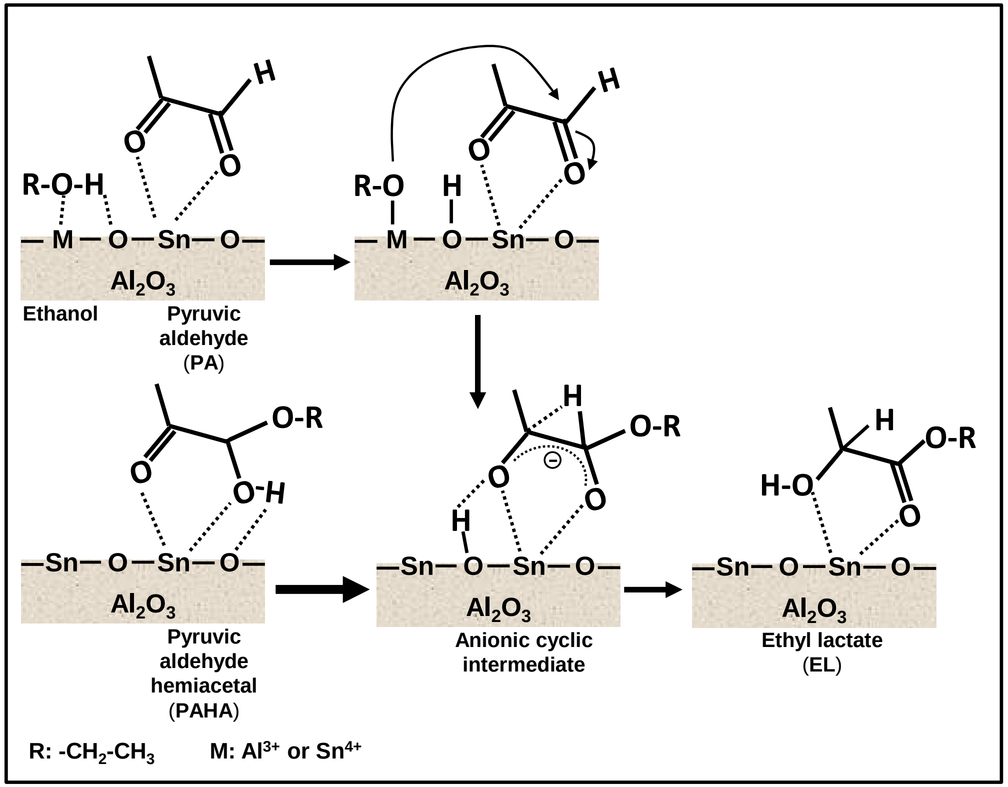

Scheme 2: Postulated surface reaction mechanism on Sn sites for EL formation by steps 3 and 6 of **Scheme 1**

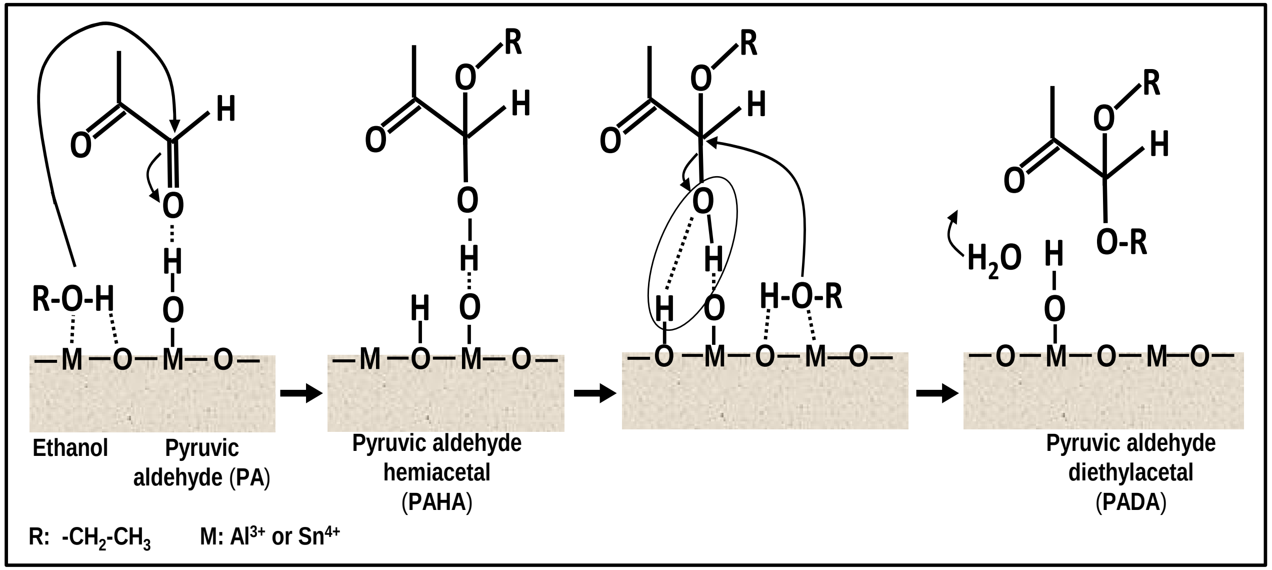

Scheme 3: Postulated surface reaction mechanism on weak Brønsted acid sites for PADA formation by steps 4 and 5 of **Scheme 1.**

Table 1. Preparation conditions and physicochemical properties of alumina-supported Sn catalysts and reference materials

Catalyst	Preparation conditions			Surface area, *SA* (m^2/g)	UV-vis DRS analysis	Acidic Properties	
	Z, Sn loading (wt. %)	Impregnating salt	Calcination temperature (K)		Band gap energy, Eg (eV)	n_a[a] (μmol/g)	N_a[a] ($\mu mol/m^2$)
1.4SnAl	1.4	$SnCl_4.5H_2O$	573	216	4.98	103	0.48
4.2SnAl	4.2	$SnCl_4.5H_2O$	573	188	4.93	121	0.64
7.6SnAl	7.6	$SnCl_4.5H_2O$	573	222	4.83	201	0.91
4.8SnAl-D-573	4.8	$SnCl_2$	573	196	5.10	135	0.69
4.0SnAl-D-773	4.0	$SnCl_2$	773	167	4.87	79	0.47
γ-Al_2O_3	-	-	773	230	-	24	0.11
7.8wt.% SnO_2-alumina	-	-	-	130[b]	3.52	-	-

[a]by TPD of NH_3; [b]*SA* of home-made SnO_2

Table 2. Catalytic results obtained on alumina-supported Sn catalysts and reference materials

Entry	Catalyst	r^0_{DHA} (mmol/h g)	TOR^0 (min^{-1})	EL/PADA at X_{DHA}= 85%	Catalytic results at t = 7h						
					P_{EL} (g EL/kg cat h)	X_{DHA} (%)	Yield (%)				
							PA	PAHA	EL	PADA	Others
1	1.4SnAl	33.8	5.5	1.8	74	85.1	13.4	2.1	16.8	9.4	43.4
2	4.2SnAl^a	46.3	6.4	1.7	176	98.4	22.5	0.3	40.6	20.1	14.9
3	7.6SnAl	68.8	5.7	2.9	298	99.4	7.5	0.1	67.8	9.1	14.9
4	4.8SnAl-D-573^a	52.1	6.4	2.6	216	98.8	15.1	0.2	49.2	15.1	19.1
5	4.0SnAl-D-773^a	26.0	5.5	3.4	115	87.7	17.8	1.2	26.1	7.6	35.0
6	γ-Al_2O_3	2.5	1.7	-	13	11.0	1.3	6.7	3.0	0.0	0.0
7	$SnCl_4.5H_2O^a$	-	-	9.6	-	99.7	2.5	0.0	82.6	8.7	5.9
8	$SnCl_2^a$	-	-	16.8	-	99.3	5.4	0.3	77.6	2.9	13.1
9	7.6SnAl^b	108.3	9.0	2.2	528	98.8	4.2	0.0	61.2	21.2	12.1

Reaction conditions: T = 353K, ethanol/DHA=43(molar), DHA/Catalyst =0.026 mol/g

^{a}DHA/Sn ≈74 (molar)

^{b}Reaction conditions: T = 373K, ethanol/DHA=43(molar), DHA/Catalyst =0.052 mol/g